J. R. Clark, W.-T. Hsu, and C. T.-C. Nguyen, "High-*Q* VHF micromechanical contour-mode disk resonator," *Technical Digest*, IEEE Int. Electron Devices Meeting, San Francisco, California, Dec. 11-13, 2000, pp. 493-496.

High-*Q* VHF Micromechanical Contour-Mode Disk Resonators

John R. Clark, Wan-Thai Hsu, and Clark T.-C. Nguyen

Center for Integrated Microsystems
Department of Electrical Engineering and Computer Science
University of Michigan
Ann Arbor, Michigan 48109-2122 USA

ABSTRACT

A micromechanical, laterally vibrating disk resonator, fabricated via a technology that combines polysilicon surface-micromachining and metal electroplating to attain submicron lateral capacitive gaps, has been demonstrated at frequencies approaching 160 MHz with *Q*'s as high as 9,400—the highest demonstrated to date for an on-chip resonator in this frequency range. This frequency also represents the highest to date for an *electrostatically transduced* micromechanical resonator and is an important step towards reaching the frequencies required by the RF front-ends in wireless transceivers. The geometric dimensions necessary to reach a given frequency are larger for this contour-mode than for the flexural-modes used by previous resonators. This, coupled with its unprecedented *Q* value, makes this disk resonator a choice candidate for use in the IF and RF stages of future miniaturized transceivers.

I. INTRODUCTION

With recent frequency increases to the mid-VHF range [1,2], vibrating micromechanical ("μmechanical") resonators with *Q*'s approaching 10,000 have emerged as leading candidates for on-chip versions of the low-loss, small percent bandwidth IF filters and the high-*Q* reference oscillator tanks required in wireless communication handsets. Having achieved the VHF frequencies needed for IF applications, μmechanical resonators now look towards the UHF frequencies needed for RF applications. As detailed in [3], it is in RF applications where μmechanical resonators are projected to make their biggest impact, as the defining elements in RF channel-select filter banks and ultra-low power, low-phase noise synthesizers, both made possible by *Q*'s >5,000, and both targeted for use in alternative transceiver architectures that trade power for *Q*.

Much like the case for transistors, extending the frequency of μmechanical resonators generally entails scaling of resonator dimensions. Some of the previous VHF demonstrations with clamped-clamped boundary conditions actually used submicron dimensions to avoid *Q*-limiting anchor losses [1]. Unfortunately, smaller size often coincides with smaller power handling [3] and an increased susceptibility to environmental effects [4], such as contamination or thermal fluctuations. Although recently demonstrated free-free beam μmechanical resonators have been able to achieve frequencies up to 92 MHz with *Q*'s around 8,000 while avoiding submicron dimensions [2], whether or not they can maintain their size and *Q* at UHF frequencies has yet to be seen.

This work presents an alternative, perhaps superior, design based on the radial contour mode, or areal dilation, of a μmechanical disk structure, and capable of attaining very high frequencies, while retaining relatively large dimensions. Using this disk design, a frequency of 156 MHz has been attained with a *Q* exceeding 9,400 and with a diameter of 34 μm—substantially larger than the 11.3 μm required to attain only 92 MHz in previous free-free beam resonators [2].

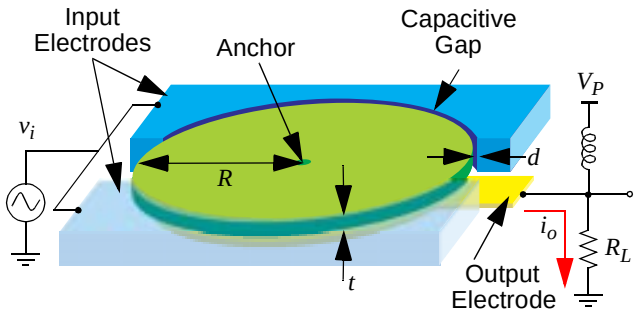

Fig. 1: Perspective view of a disk microresonator illustrating a preferred one-port bias and excitation scheme.

II. RESONATOR OPERATION

Figure 1 presents the perspective-view schematic of the disk μresonator, identifying key dimensions and indicating a preferred bias and excitation scheme. The resonator consists of a disk suspended 5,000 Å above the substrate with a single anchor at its center. Plated metal input electrodes surround the perimeter of the disk, separated by a narrow air (or vacuum) gap that defines the capacitive, electromechanical transducer of this device. As illustrated, two split electrodes surround the disk in order to allow routing to the structure while maintaining a symmetric distribution of electrostatic force. (In Fig. 1, the front electrode is rendered partially transparent to enable the reader to view the underlying structure.) To operate the device, a DC bias voltage V_P is applied to the structure, while an AC input signal is applied to the electrodes, resulting in a time varying electrostatic force acting radially on the disk. When the input signal, and hence the force that it generates, are acting at the resonant frequency of the device, that force is multiplied by the *Q* factor of the resonator, producing expansion and contraction of the disk along its radius. This motion, in turn, results in a time-varying, DC-biased capacitor between the disk and the electrodes generating an output current given by

$$i_o = V_P \frac{\partial C}{\partial x}\frac{\partial x}{\partial t}, \qquad (1)$$

where *x* is the radial displacement at the edge of the disk and $\partial C/\partial x$ is the change in electrode-to-resonator overlap capacitance per unit displacement. The output current i_o can be sensed either directly as the voltage across the load resistor R_L, or via a transimpedance amplifier. Note that if resonator *Q* is the primary measurement parameter, the load resistance R_L should be kept small in order to minimize *Q*-loading.

As shown in previous work on free-free beam μmechanical resonators, resonators with relatively large dimensions exhibit higher stiffnesses than their submicron counterparts,

and thus, can achieve high Q only if sufficiently isolated from the substrate so as to eliminate energy losses to it. In the particular free-free beam design of [2], isolation from the substrate was achieved in part by attaching support beams only at flexural-mode nodal points. The disk design of this work very conveniently allows a similar isolation strategy. In particular, the motion of the disk is symmetric and purely radial at the desired resonance, so its center corresponds to a motionless nodal point during vibration. Anchoring the resonator at its center, as shown in Fig. 1, then minimizes energy losses to the substrate, allowing high-Q operation despite the high stiffness of this design.

III. DISK RESONATOR DESIGN

To facilitate the incorporation of disk resonators into filter and oscillator designs, equivalent circuit models and analytical formulations for resonator properties (e.g., resonant frequency, impedance) are needed. These are now addressed.

A. Frequency Design

The mechanical resonant frequency for the radial contour mode of a disk is governed mainly by its material properties and its radius. Neglecting second order effects due to thickness and finite anchor dimensions, the resonant frequency may be determined by finding a numerical solution for f_o to the system of equations [5]

$$\frac{J_0(\zeta/\xi)}{J_1(\zeta/\xi)} = 1-\sigma\,, \tag{2}$$

$$\zeta = 2\pi f_o R\sqrt{\frac{\rho(2+2\sigma)}{E}}\,, \tag{3}$$

$$\xi = \sqrt{\frac{2}{1-\sigma}}\,, \tag{4}$$

where R is the radius of the disk; E, σ, and ρ are the Young's modulus, Poisson's ratio, and density, respectively, of its structural material; and $J_n(y)$ is the Bessel function of the first kind of order n.

While representing a rigorous solution to the differential equations of vibration, this set of equations does not provide clear insight into how the individual parameters affect the frequency. By sacrificing some degree of accuracy, (2)-(4) can be rendered into the more intuitive form,

$$f_o = \frac{\alpha}{R}\sqrt{\frac{E}{\rho}}\,, \tag{5}$$

where α is a parameter dependent upon Poisson's ratio and the desired mode shape. (α = 0.342 for polysilicon in the mode shape used here [6].) From (5), the resonant frequency of a disk is inversely proportional to its radius. Figure 2 plots resonant frequency versus diameter for polysilicon disks, showing that even at the 900-1800 MHz RF frequencies commonly used in wireless handsets, the required diameters of 6.2 μm for 900 MHz and 3 μm for 1.8 GHz are well within the capabilities of present-day integrated circuit fabrication technology.

B. Electrical Equivalent Circuit

Figure 3 presents the equivalent *RLC* circuit modeling the disk resonator of Fig. 1 along with equations for its circuit elements. In this circuit, the motional elements R_x, L_x, and C_x model the resonant behavior of the device, while the capacitor C_o models the static capacitance between the electrode and disk. The values of the *RLC* circuit elements are

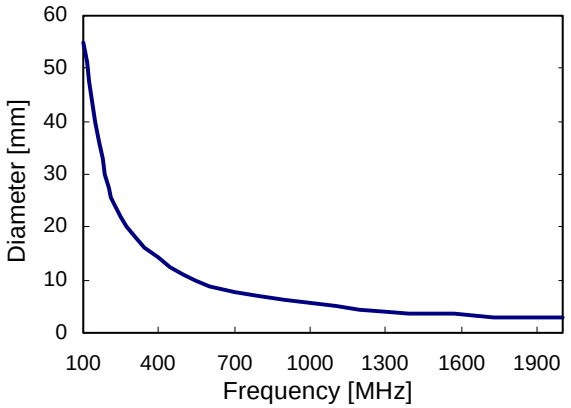

Fig. 2: Plot of diameter vs. frequency for a polysilicon disk.

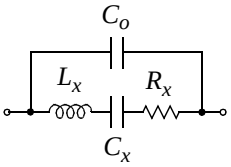

$$C_x = \frac{\eta^2}{k_r} \qquad R_x = \frac{\sqrt{k_r m_r}}{Q\eta^2}$$

$$L_x = \frac{m_r}{\eta^2} \qquad \eta = V_P\frac{\partial C}{\partial x}$$

Fig. 3: Schematic of the electrical equivalent circuit of a disk resonator, including equations for the component values.

dependent on the Q of the resonator, the electromechanical coupling coefficient η, and the effective mass m_r and stiffness k_r of the resonator, given by

$$m_r = \frac{\rho\pi t}{4hJ_1(hR)}\int_0^R hJ_1(hr)\partial r\,, \tag{6}$$

$$k_r = \omega_o^2 m_r\,, \tag{7}$$

$$h = \sqrt{\frac{\omega^2\rho}{\frac{2E}{2+2\sigma}+\frac{E\sigma}{1-\sigma^2}}}\,, \tag{8}$$

where $\omega_o=2\pi f_o$, and t is the thickness of the resonator. Note that the effective mass of a radial contour mode disk is independent of location, indicating that all points on the circumference of the disk are moving with the same velocity and obviating the complex integration required to obtain accurate circuit parameters in flexural mode counterparts [7].

In many applications, the series motional resistance R_x must often be minimized for impedance matching purposes. According to the equations in Fig. 3, and assuming that Q is fixed, this is best done by maximizing the dc-bias voltage V_P and the $\partial C/\partial x$ term. In many practical systems, however, the maximum voltage is often limited by either the transistor technology supporting the resonator or the available power supply, leaving $\partial C/\partial x$, which varies as (t/d^2), as the only adjustable parameter. Thickness t is limited by technology constraints and by second order effects that cause frequency to decrease as thickness increases, so $\partial C/\partial x$ is best increased by decreasing the electrode-to-resonator gap spacing d. Since $\partial C/\partial x$ varies as $(1/d^2)$, changes in d have a very strong effect on R_x, which from Fig. 3 should vary as $(1/d^4)$. To illustrate the importance of d, a 200 MHz resonator with d=1 μm, t=2 μm, and V_P=20 V has an R_x=286 MΩ, which is very high, especially at RF frequencies. If the gap is reduced to 1000 Å while maintaining the other parameters, R_x decreases to 29 kΩ—strong justification for a disk resonator fabrication

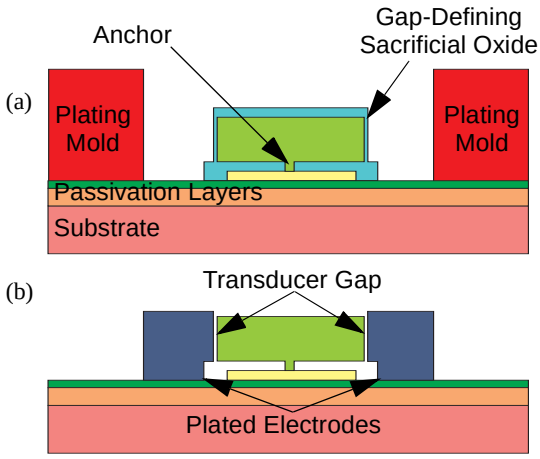

Fig. 4: Process cross section of a disk resonator. (a) A conformal oxide and electroplating mold are added to the a surface micromaching process. (b) Electrode is plated between the PR mold and sidewalls, then the structure is released.

technology capable of realizing submicron lateral electrode-to-resonator gaps, such as that described in Section IV.

IV. FABRICATION

The need for submicron, high-aspect ratio, lateral electrode-to-resonator gaps in the disk resonator of Fig. 1 constitutes the most daunting requirement on the fabrication technology. Although 1000 Å lateral gaps have been achieved previously in μmechanical structures using e-beam lithography [8], this approach was found to be both time consuming and costly. In addition, if impedances on the order of 50Ω are desired, 1000 Å gaps may not be sufficient, and even smaller gaps on the order of 300 Å may in fact be desired [9]. To avoid the limitations of lithography and dry etching, the fabrication technology of this work combines surface micromachining, metal electroplating, and a sacrificial sidewall-spacer technique to achieve lateral polysilicon disk resonators with metal electrodes and submicron lateral electrode-to-resonator gaps, all without the need for aggressive lithographic or etching capability.

Figure 4 presents a pair of cross sections from the process flow. The initial process steps are identical to those used in previous polysilicon surface micromaching processes [7] to achieve a cross-section where a 2 μm-thick polysilicon layer, patterned to form the disk structure, is temporarily supported by a 5000 Å first sacrificial oxide layer. Instead of releasing the structure at this point, as would be done in a conventional surface micromachining process, this process continues with the conformal deposition of 1000 Å of LPCVD oxide to cover the sidewalls of the structure and serve as the gap-defining sacrificial layer. Next, the sacrificial oxide and the underlying oxide are etched to open anchors to the passivation layers, and a metal seed layer is evaporated onto the wafer and removed from the top and sides of the structure in order to prevent plating in these areas. A thick photoresist mold is then deposited and patterned to define the electrodes, resulting in the cross-section of Fig. 4(a). This is followed by plating of the electrodes, using the PR as one portion of the mold and the sidewall of the structure as the other, plating directly against the sacrificial oxide layer. The PR and seed layer are then stripped, and the structure is released in HF to achieve the final cross-section shown in Fig. 4(b). The result: A disk suspended over the substrate by a single anchor in the middle, and separated from the plated electrodes by a thin air gap defined by the sacrificial layer. The minimum gap thickness in this process is limited only by the ability to control the thickness of a conformally deposited oxide film, and is independent of lithography and etching. Figure 5 presents a wide-view scanning electron micrograph (SEM) of a fabricated and released 156 MHz disk resonator. Figure 6 shows a zoom-in SEM of this same resonator, offering a clearer view of its 1000 Å electrode-to-resonator gap.

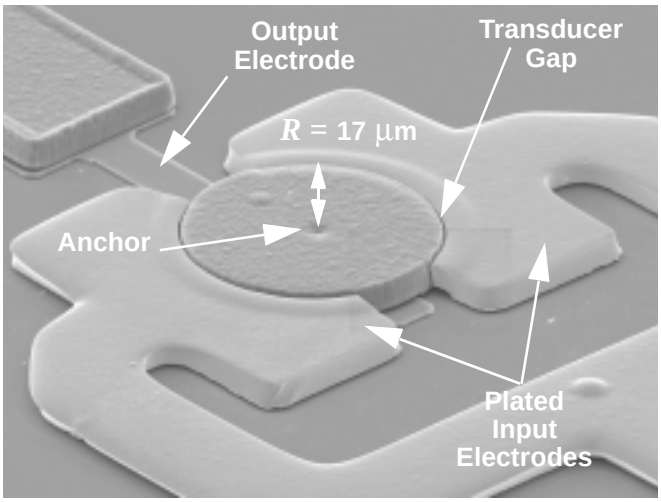

Fig. 5: SEM of a fabricated and released 156 MHz disk μmechanical resonator.

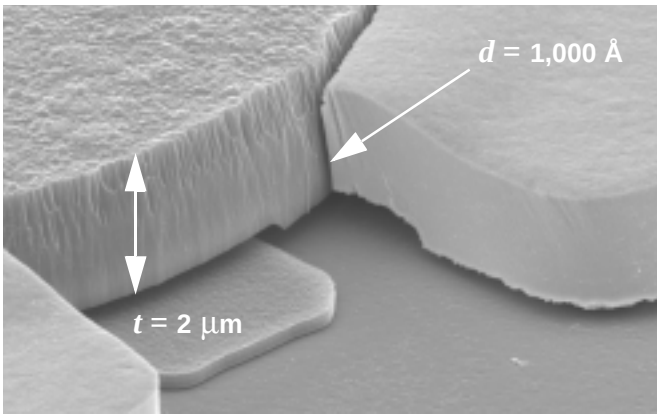

Fig. 6: Zoomed SEM of a 156 MHz disk μmechanical resonator, giving a clearer view of its 1000Å electrode-to-resonator gap.

V. EXPERIMENTAL RESULTS

Completed disk resonators were tested in a custom-built vacuum chamber capable of pressures on the order of 50 μTorr and fitted with feedthroughs to allow electrical connections between an inserted printed circuit board (housing the disk resonator die) and external measurement instrumentation. An HP 8753A Network Analyzer was used to attain resonator frequency spectra.

Figure 7 depicts a commonly used setup for directly measuring the transmission spectrum (v_i/i_o) of a one-port micromechanical resonator using the circuit of Fig. 1. Here, the 50Ω impedance of the network analyzer detection port serves as the R_L that detects the resonator output current i_o. The frequency spectrum for a 156 MHz resonator, measured

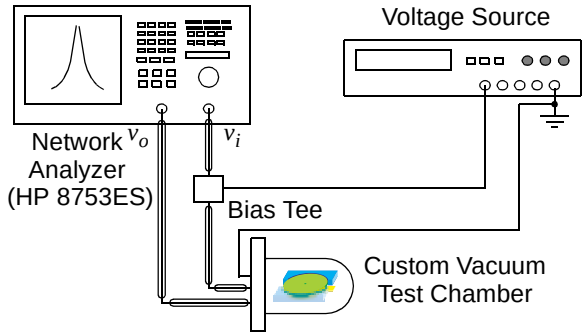

Fig. 7: Test set-up for measuring the frequency characteristic of a one-port μmechanical resonator.

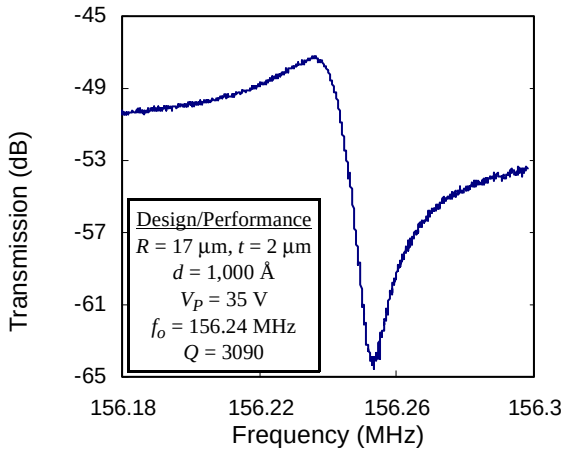

Fig. 8: Transmission spectrum for the 156 MHz disk resonator measured using the set-up in Fig. 7.

using this setup, is shown in Fig. 8, from which a Q of 3,090 is extracted. However, this particular measurement set-up does very little to suppress high frequency parasitic feedthrough currents that visibly interfere with the measurement and decrease the size of the series resonant peak in Fig. 8, so this Q value represents only a conservative estimate of the true device Q.

Perhaps the simplest solution to this problem is to increase the dc-bias voltage V_P from 35V to 70V, which, according to the equation in Fig. 3, should decrease R_x by 4X and hence increase the motional current by this same factor, raising the resonant peak of Fig. 8 by 12 dB above the feedthrough. Unfortunately, the dc-bias on the structure could not be raised past 35V, due to a problem with shorting between the resonator and its electrodes when V_P's >35V are applied. Although not proven, one possible mechanism behind this shorting phenomenon is bending of the soft metal electrode under the large electrostatic forces generated by large V_P's. An alternative Au plating solution is being explored to achieve more rigid electrodes in hopes of removing this V_P limitation.

In the meantime, feedthrough problems can also be mitigated by making measurements using the set-up of Fig. 9, where the resonator of Fig. 1 is now operated as a two-port device, with its two electrodes serving as input and output terminals, and with V_P applied directly to the disk without a bias tee. In this configuration, the feedthrough capacitance C_o of Fig. 3 is now effectively split into two shunt capacitors to ground, substantially reducing parasitic feedthrough, and thus, allowing measurement of the curve in Fig. 10. Here, the

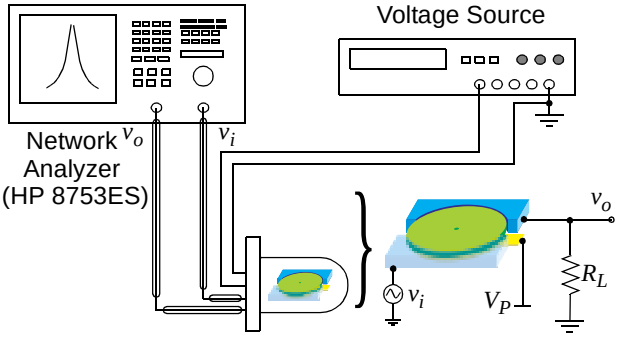

Fig. 9: Test set-up for measuring the frequency characteristic of a two-port μmechanical resonator.

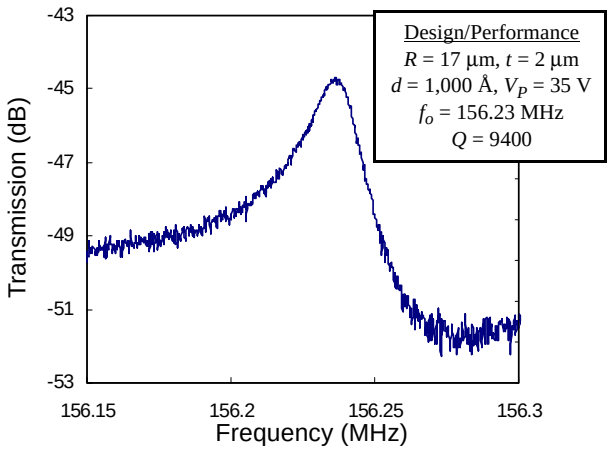

Fig. 10: Transmission spectrum for the 156 MHz disk resonator measured using the set-up in Fig. 9.

resonant peak is high enough to obtain a more accurate estimate of Q=9,400—a very impressive value at 156 MHz.

VI. CONCLUSIONS

A laterally vibrating radial contour mode μmechanical disk resonator was presented with a measured frequency and Q of 156 MHz and 9,400, respectively—the highest to date for electrostatically driven μmechanical resonators. Although already ground-breaking, this result is most likely only a precursor to even higher UHF frequencies to come (e.g., 900 MHz), which, as shown in this paper, should be achievable via this design with very reasonable geometric dimensions. If disk resonators at these frequencies can maintain Q's around 10,000, then revolutionary signal processor concepts with substantial potential for lowering power consumption in wireless handsets (e.g., an RF channel selector at the front-end of a wireless receiver) may become more plausible in the near future. Frequency extension of μdisks continues.

***Acknowledgment*:** This work was supported under DARPA Cooperative Agmt. No. F30602-97-2-0101.

References:

[1] M. Roukes, *Hilton Head'2000*, pp. 367-376.
[2] K. Wang, *et al.*, *MEMS '99*, pp. 453-458.
[3] C. T. Nguyen, *IEEE Trans. MTT*, pp. 1486-1503, Aug. 1999.
[4] J. R. Vig, *et al.*, *IEEE Trans.UFFC*, pp. 1558-1565, Nov. 1999.
[5] M. Onoe, *J. Accoust. Soc. Amer.*, pp. 1158-1162, Nov. 1956.
[6] R. A. Johnson, *Mechanical Filters in Electronic*s, Wiley, 1983.
[7] F. Bannon, *et al.*, *IEEE JSSC*, pp. 512-526, April 2000.
[8] J. Weigold, *et al.*, *IEEE JMEMS*, pp. 221-228, Sept. 1999.
[9] A.-C. Wong, *et al.*, *IEDM'98*, pp. 471-474.